The role of caking in optimising the performance of a concertinaed ceramic filtration membrane

Victoria E. Pereira, Mohit P. Dalwadi, Ian M. Griffiths

September 14, 2021

Abstract

Membrane filtration is a process of separating particles from fluids. Over time, particles are trapped within the membrane structure and on the membrane surface, forming a *cake*. In this paper, we develop a mathematical model for the transient blocking dynamics in a concertinaed filtration device composed of angled porous membranes and dead-ends. We examine how the inclusion of particles affects the flow dynamics, and we uncover potential inaccuracies in relying on flux–throughput curves to distinguish between caking and internal blocking dynamics. Moreover, we show that optimal filtration performance depends strongly depends on both the performance metric and the membrane configuration. Finally we introduce a method for deriving a non-uniform permeance that ensures constant initial cake growth.

1   Introduction

Membrane filtration is a vital process used to separate fluid mixtures in many industry sectors including healthcare, water treatment, and food production [Noble and Stern, 1995; van Reis and Zydney, 2007; Yao et al., 1971]. Filtration devices comprise porous membranes through which a mixture of fluid and unwanted particles is passed. The particles get trapped by the membrane and a filtered fluid is produced. While efficient instantaneous trapping of unwanted particles makes for a good filter, this occurs at the cost of blocking the filter over time, which can reduce the total amount of fluid processed by the device. There are two key blocking mechanisms: blocking inside the membrane pores (internal blocking) and blocking on the surface of the membrane (caking).

There are a wide range of filtration devices and in this paper we focus our attention to *direct-flow* filtration devices. Such devices consist of stacked porous membranes with alternating capped ends (see figure 1a). The fluid mixture is passed into the device through open ends, travels through the porous membrane and out through the other side through open ends. Typically, in direct-flow devices, the fluid is fed in parallel to the membrane surface. In this paper, we seek to understand how filtration performance is affected by an angled-membrane configuration in a direct-flow device. The motivation for this study arises from an industrial example of such a direct-flow device designed by Smart Separations Ltd. The steady-state version of

the model presented herein is derived in earlier work [Pereira et al., 2021]. The goal of the previous study was to optimise the filtration performance for a particle-free steady flow. In this paper we build on this previous work to incorporate transient blocking effects in the optimisation of the performance of a concertinaed filtration system.

An understanding of the blocking dynamics in filtration is vital in optimising the design of a filter, and there have been a number of previous studies of examining such dynamics. Wang et al. [2017] developed a mathematical model of internal blocking in vertically stacked filtration membranes in a direct-flow device. This previous study looked at the effect of spacing between the membranes on the total amount of fluid processed through the device. Further relevant work arises from studies of blocking in pleated filtration membranes, which are geometrically similar to a direct-flow device with the key difference being the presence of dead ends in the latter. King and Please [1996] presented an asymptotic analysis of caking dynamics relevant for several different parameter regimes applied to a rectangularly pleated device. Later work by Sanaei et al. [2016] incorporated both caking and internal-blocking dynamics in a mathematical model of flow through a rectangular pleated membrane with surrounding porous support material. The work sought to examine the relative importance of the resistance of the support material to that of the membrane, and the evolution of the permeability profile through internal blocking. Recently, Sun et al. [2020] presented a model of internal blocking within an analogous device of rectangular pleats contained in porous support material. The authors compared linear, quadratic, and cubic membrane permeability profiles with the aim of maximising the total amount of fluid processed through the filtration device.

In this paper we present a mathematical model of caking dynamics in a direct-flow device with angled membranes. The distinction between the past works of blocking dynamics in a filtration device and the work presented in this paper is that we focus our study on the effects of particle inclusion, membrane configuration (namely angle and position), and membrane permeability profile on the caking dynamics in a concertinaed filtration device.

2 Model development

In this paper, we consider the flow through a single repeated module of the filtration device shown in figure 1. The geometry of the device is such that the transverse length $\hat{X}$ is significantly smaller than the lateral length $\hat{Z}$ and depth $\hat{Y}$ (see table 1). Moreover, variations in the $\hat{y}$-axis are assumed to be negligible, and we consider the two-dimensional domain in $(\hat{x}, \hat{z})$-space (see figure 1b). We will derive the model using dimensional quantities (denoted by hats) and then scale the model to derive the associated dimensionless quantities (denoted without hats). The position of the upstream side of the membrane is specified by $\hat{x} = \hat{m}(\hat{z})$ with

$$\hat{m}(\hat{z}) = \hat{a} + \tfrac{1}{2}\left(\hat{Z}\tan\hat{\beta} - \hat{h}\right) - \hat{z}\tan\hat{\beta}, \tag{2.1}$$
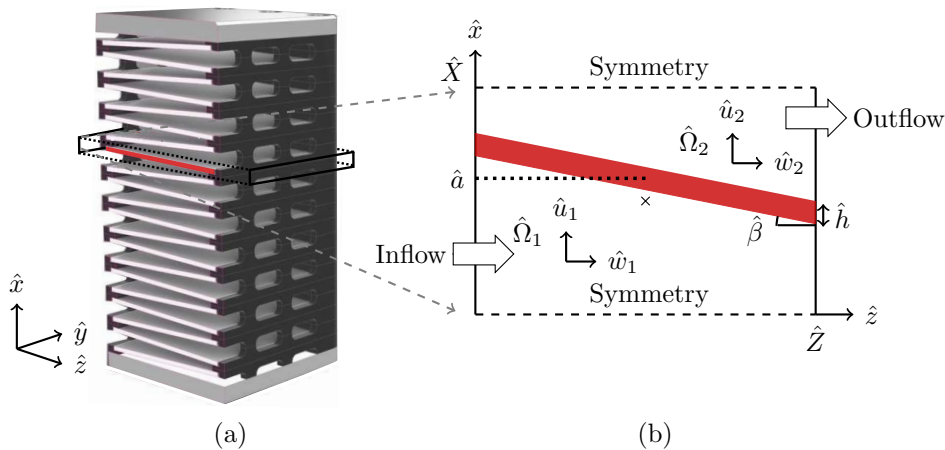
Figure 1: Schematic of the concertinaed filtration device. Figure 1a shows the full three-dimensional device; reproduced from Smart Separations Ltd [2020] with permission. Figure 1b depicts the two-dimensional domain of a single filtration module; the centre of the membrane is $(\hat{x}, \hat{z}) = (\hat{a}, \hat{Z}/2)$ and the centre of the domain $(\hat{x}, \hat{z}) = (\hat{X}/2, \hat{Z}/2)$ is indicated by a cross.

where $\hat{\beta}$ is the angle of the membrane with the horizontal axis and $\hat{h}$ is the membrane thickness (see figure 1b). The membrane length $\hat{L} = \hat{Z}/\cos\hat{\beta}$ is governed by the angle $\hat{\beta}$. The position of the membrane midpoint $(\hat{x}, \hat{z}) = (\hat{a}, \hat{Z}/2)$ is determined through the parameter $\hat{a}$. The membrane separates the flow domain into two subdomains described by

$$\hat{\Omega}_1 = \{\hat{x} \in [0, \hat{s}(\hat{z}, \hat{t})], \hat{z} \in [0, \hat{Z}]\}, \tag{2.2a}$$

$$\hat{\Omega}_2 = \{\hat{x} \in [\hat{m}(\hat{z}) + \hat{h}, \hat{X}], \hat{z} \in [0, \hat{Z}]\}, \tag{2.2b}$$

where $\hat{x} = \hat{s}(\hat{z}, \hat{t})$ is the position of the moving cake front at time $\hat{t}$.

Driven by a pressure drop $(\hat{p}_{\text{in}} - \hat{p}_{\text{out}}) > 0$, where $\hat{p}_{\text{in}}$ and $\hat{p}_{\text{out}}$ are the inlet and outlet pressures respectively, the flow enters the domain $\hat{\Omega}_1$ at $\hat{z} = 0$, travels into the cake at $x = s(z, t)$, through to the membrane at $\hat{x} = \hat{m}(\hat{z})$, and exits the domain $\hat{\Omega}_2$ at $\hat{z} = \hat{Z}$. The fluid mixture comprises liquid and particles to be filtered.

The steady-state flow studied in our previous paper [Pereira et al., 2021] is reversible and the results for $\hat{\beta} > 0$ can generalised to those for $\hat{\beta} < 0$ with the subdomains $\hat{\Omega}_1$ and $\hat{\Omega}_2$ switched for symmetric flux. However, in this paper we consider the transient system with an evolving cake front in which the flow is not reversible and as such we cannot obtain the results for $\hat{\beta} < 0$ from the $\hat{\beta} > 0$ setup. We note, however, that, when $\hat{\beta} < 0$, as $|\hat{\beta}|$ is increased, the size of the inlet decreases which has the effect of increased pressure drop in $\hat{\Omega}_1$ and thus a reduced pressure drop across the membrane. This consequently decreases the flux through the device. In this paper, we seek a filter configuration that maximises the processed fluid volume and we will therefore restrict our attention to $\hat{\beta} \geq 0$.

3

Parameter	Value
Lateral height, $\hat{Z}$	50 mm
Filter depth, $\hat{Y}$	50 mm
Transverse length, $\hat{X}$	3.6 mm
Air viscosity, $\hat{\mu}$	1.81×10^{-5} Pa s
Air density, $\hat{\rho}$	1.2 kg m^{-3}
Lateral velocity scale, $\hat{W}_0$	50 mm s^{-1}

Table 1: Parameter values for air flow through the filtration device shown in figure 1; values for $\hat{Z}$, $\hat{Y}$, $\hat{X}$, and $\hat{W}_0$ provided by Smart Separations Ltd [2020].

2.1 Governing equations

The multiphase flow comprises a continuous fluid phase and discrete particles; the phase distribution is described through the corresponding volume fractions ϕ^f, ϕ^p. We assume the particles to be sufficiently small so as to not disturb the dynamics of the continuous fluid flow. The flow dynamics of both phases (fluid and particles) can therefore be described by a single velocity $\hat{\boldsymbol{u}}(\hat{x}, \hat{z}, \hat{t}) = (\hat{u}(\hat{x}, \hat{z}, \hat{t}), \hat{w}(\hat{x}, \hat{z}, \hat{t}))$ and pressure $\hat{p}(\hat{x}, \hat{z}, \hat{t})$. We assume there to be a constant volume fraction of particles in $\hat{\Omega}_1$:

$$\phi^p = \phi_1^p \quad \text{in} \quad \hat{\Omega}_1. \tag{2.3}$$

The fluid volume fraction $\phi_1^f = 1 - \phi_1^p$ is therefore also constant. In the subdomain $\hat{\Omega}_2$ we assume that no particles are present:

$$\phi_2^p = 0, \quad \text{in} \quad \hat{\Omega}_2. \tag{2.4}$$

Hence, the fluid volume fraction in $\hat{\Omega}_2$ is $\phi_2^f = 1$. While (2.4) assumes perfect filtration of the particles, we note that it is straightforward to extend this model to account for imperfect filtering with $\phi_2^p \neq 0$.

The geometry of the system is such that the ratio between the transverse and lateral domain lengths $\epsilon = \hat{X}/\hat{Z}$ is small. Indeed, ϵ is sufficiently small to result in a small reduced Reynolds number $\epsilon^2 \text{Re} = \epsilon^2 \hat{\rho} \hat{W}_0 \hat{Z}/\hat{\mu}$ (see Table 1). The flow in $\hat{\Omega}_1$ and $\hat{\Omega}_2$ is thus modelled through the Stokes equations:

$$\hat{\mu} \hat{\boldsymbol{\nabla}}^2 \hat{\boldsymbol{u}} - \hat{\boldsymbol{\nabla}} \hat{p} = 0, \tag{2.5a}$$
$$\hat{\boldsymbol{\nabla}} \cdot \hat{\boldsymbol{u}} = 0, \tag{2.5b}$$

where $\hat{\mu}$ is the fluid viscosity, which we assume to be constant. We seek solutions $(\hat{u}_1, \hat{w}_1, \hat{p}_1)$ in $\hat{\Omega}_1$ and $(\hat{u}_2, \hat{w}_2, \hat{p}_2)$ in $\hat{\Omega}_2$.

The boundary conditions at the inlet and outlet are

$$\hat{p}_1 = \hat{p}_{\text{in}} \quad \text{at } \hat{z} = 0, \ \hat{x} \in [0, \hat{s}(0, \hat{t})], \tag{2.6a}$$
$$\hat{p}_2 = \hat{p}_{\text{out}} \quad \text{at } \hat{z} = \hat{Z}, \ \hat{x} \in [\hat{m}(\hat{Z}) + \hat{h}, \hat{X}]. \tag{2.6b}$$

4

At the closed ends in both subdomains, at $\hat{z} = \hat{Z}$ in $\hat{\Omega}_1$ and at $\hat{z} = 0$ at $\hat{\Omega}_2$, we prescribe no-flow boundary conditions:

$$\hat{\boldsymbol{u}}_1 = \boldsymbol{0} \quad \text{at } \hat{z} = \hat{Z}, \quad \hat{x} \in [0, \hat{s}(\hat{Z}, \hat{t})], \tag{2.7a}$$

$$\hat{\boldsymbol{u}}_2 = \boldsymbol{0} \quad \text{at } \hat{z} = 0, \quad \hat{x} \in [\hat{m}(0) + \hat{h}, \hat{X}]. \tag{2.7b}$$

We assume symmetric flow between neighbouring modules, which corresponds to the following symmetry conditions:

$$\hat{u}_1 = 0, \quad \frac{\partial \hat{w}_1}{\partial \hat{x}} = 0 \quad \text{at } \hat{x} = 0, \tag{2.8a}$$

$$\hat{u}_2 = 0, \quad \frac{\partial \hat{w}_2}{\partial \hat{x}} = 0 \quad \text{at } \hat{x} = \hat{X}. \tag{2.8b}$$

The porous membrane and cake layers provide resistance to the flow. In general, the flow resistance $\hat{R}$ due to a permeable material of thickness $\hat{h}$ and permeability $\hat{k}$ is the reciprocal of the permeance $\hat{\kappa} = \hat{k}/\hat{\mu}\hat{h}$: $\hat{R} = 1/\hat{\kappa}$. In our problem, the total resistance is the sum of the resistance of the membrane $\hat{R}_m$ and that of the cake layer $\hat{R}_c$:

$$\hat{R}(\hat{z}, \hat{t}) = \hat{R}_m + \hat{R}_c(\hat{z}, \hat{t}) = \frac{\hat{\mu}\hat{h}}{\hat{k}_m} + \frac{\hat{\mu}(\hat{m}(\hat{z}) - \hat{s}(\hat{z}, \hat{t}))}{\hat{k}_c}, \tag{2.9}$$

where $(\hat{m}(\hat{z}) - \hat{s}(\hat{z}, \hat{t}))$ is the cake thickness, and $\hat{k}_m$ and $\hat{k}_c$ are the permeabilities of the membrane and cake layer, respectively. Thus we see that the total permeance is

$$\hat{\kappa}(\hat{z}, \hat{t}) = \left[\frac{\hat{\mu}\hat{h}}{\hat{k}_m} + \frac{\hat{\mu}(\hat{m}(\hat{z}) - \hat{s}(\hat{z}, \hat{t}))}{\hat{k}_c} \right]^{-1}. \tag{2.10}$$

The permeance and pressure difference govern the flow through the porous membrane and cake layers. We impose Darcy flow across the membrane and cake, which provides the outflow boundary condition in $\hat{\Omega}_1$. This boundary condition is prescribed on $\hat{x} = \hat{s}(\hat{z}, \hat{t})$, which corresponds initially to the membrane surface, $\hat{s}(\hat{z}, 0) = \hat{m}(\hat{z})$, and on the cake front, $\hat{s}(\hat{z}, \hat{t})$, at later times $\hat{t} > 0$. The Darcy boundary condition is therefore given by

$$\hat{\boldsymbol{u}}_1 \cdot \boldsymbol{n}_s = \hat{\kappa}(\hat{z}, \hat{t}) \left[\hat{p}_1(\hat{s}, \hat{z}, \hat{t}) - \hat{p}_2(\hat{m} + \hat{h}, \hat{z}, \hat{t}) \right] \quad \text{at } \hat{x} = \hat{s}(\hat{z}, \hat{t}), \tag{2.11}$$

where $\boldsymbol{n}_s$ is the unit normal vector to the cake front.

The corresponding boundary condition for the flow velocity into $\hat{\Omega}_2$ from the membrane is given by balancing the flux of fluid through the cake and membrane:

$$\phi_1^f \hat{\boldsymbol{u}}_1(\hat{s}, \hat{z}, \hat{t}) = \hat{\boldsymbol{u}}_2(\hat{m} + \hat{h}, \hat{z}, \hat{t}). \tag{2.12}$$

Finally, to close the system of equations, we prescribe no slip on both sides of the membrane:

$$\hat{\boldsymbol{u}}_1 \cdot \boldsymbol{t}_s = 0 \quad \text{at } \hat{x} = \hat{s}(\hat{z}, \hat{t}), \tag{2.13a}$$

$$\hat{\boldsymbol{u}}_2 \cdot \boldsymbol{t}_m = 0 \quad \text{at } \hat{x} = \hat{m}(\hat{z}) + \hat{h}, \tag{2.13b}$$

where $\boldsymbol{t}_s$ and $\boldsymbol{t}_m$ are, respectively, the unit tangent vectors to the cake front and membrane. While previous work by Beavers and Joseph [1967] describes the appropriate tangential slip-flow boundary condition, subsequent work by Griffiths et al. [2013] has shown that the inclusion of slip does not significantly affect the flow dynamics and we therefore neglect slip effects here.

2.2 Caking dynamics

The model equations presented so far describe the flow dynamics in the subdomains $\hat{\Omega}_1$ and $\hat{\Omega}_2$. In general there are two key blocking mechanisms in filtration systems: internal blocking and caking. Typically, small particles are filtered out within the membrane depth via internal blocking, while large particles that cannot penetrate into the membrane form a cake layer on the surface. Experimental studies conducted by Smart Separations Ltd [2020] indicated that, for the particular application of filtering dust from air, caking is more prominent than internal blocking, and we therefore focus our study on caking dynamics.

The cake-evolution equation follows from conservation of flux across the moving cake front:

$$\frac{\partial \hat{s}/\partial \hat{t}}{\sqrt{1 + (\partial \hat{s}/\partial \hat{z})^2}} = -\phi_1^p \gamma_c \hat{\boldsymbol{u}}_1(\hat{s}, \hat{z}, \hat{t}) \cdot \boldsymbol{n}_s \tag{2.14}$$

where the left-hand side is the normal velocity to the moving cake front (see Appendix A for derivation). We have introduced the packing coefficient $\gamma_c = (\phi_c^p - \phi_1^p)^{-1}$ which relates the actual volume of particles in the fluid to the volume of cake they produce, where ϕ_c^p is the volume fraction of particles in the cake layer. Note that $\gamma_c > 0$ as we have $\phi_c^p > \phi_1^p$. As noted, initially there will be no cake present:

$$\hat{s}(\hat{z}, 0) = \hat{m}(\hat{z}). \tag{2.15}$$

2.3 Dimensionless model

We introduce the following dimensionless variables:

$$\hat{t} = \tau_c t, \quad \hat{z} = \hat{Z}z, \quad \hat{x} = \epsilon \hat{Z}x, \quad \hat{\beta} = \epsilon \beta, \quad \hat{s} = \hat{X}s, \quad \hat{m} = \hat{X}m, \quad \hat{a} = \hat{X}a,$$

$$\hat{h} = \hat{X}h, \quad \hat{u} = \epsilon \hat{W}_0 u, \quad \hat{w} = \hat{W}_0 w, \quad \hat{p} = \frac{\hat{\mu}\hat{W}_0}{\epsilon^2 \hat{Z}}p + \hat{p}_{\text{out}},$$

$$\hat{\kappa} = \frac{\epsilon^3 \hat{Z}}{\hat{\mu}}\kappa, \quad \hat{\kappa}_m = \frac{\epsilon^3 \hat{Z}}{\hat{\mu}}\kappa_m, \quad \hat{k}_c = \epsilon^3 \hat{Z}\hat{X}k_c, \tag{2.16}$$

where $\tau_c = \hat{Z}/\gamma_c \hat{W}_0$ is the caking timescale, derived from the cake-evolution equation (2.14). Recalling the definition of $\gamma_c = (\phi_c^p - \phi_1^p)^{-1}$, we see that changing the volume fraction of particles in the system correspondingly changes the timescale τ_c given above. Moreover, from (2.16) we can write the velocity scaling in terms of the pressure drop: $\hat{W}_0 = \epsilon^2 \hat{Z}(\hat{p}_{\text{in}} - \hat{p}_{\text{out}})/\hat{\mu}$.

Note that the membrane angle has been scaled such that $\beta \in [0, 1]$. Applying (2.16) to (2.1) yields the dimensionless leading-order membrane position:

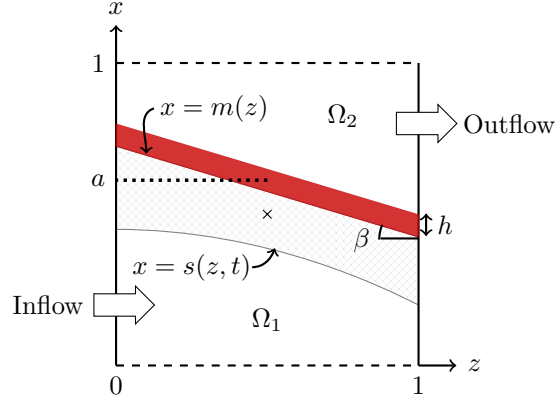$$m(z) = a - \tfrac{1}{2}h + \beta \left(\tfrac{1}{2} - z\right). \tag{2.17}$$

Figure 2: Dimensionless filtration-module domain $(x, z) \in \{[0, 1] \times [0, 1]\}$. The membrane and cake layers are schematised in red and grey, respectively, with the evolved cake front denoted by $x = s(z, t > 0)$. The membrane centre is at $(x, z) = (a, 1/2)$ and is specified by the parameter a. The membrane angle is given by β.

Applying the scalings (2.16) to (2.2) yields the following dimensionless subdomains (shown in figure 2):

$$\Omega_1 = \{x \in [0, s(z, t)], \ z \in [0, 1]\}, \tag{2.18a}$$
$$\Omega_2 = \{x \in [m(z) + h, 1], \ z \in [0, 1]\}. \tag{2.18b}$$

Scaling the Stokes equations (2.5) using (2.16) and taking the limit $\epsilon \to 0$ yields the dimensionless lubrication equations:

$$\frac{\partial p}{\partial x} = 0, \qquad \frac{\partial^2 w}{\partial x^2} - \frac{\partial p}{\partial z} = 0, \qquad \frac{\partial u}{\partial x} + \frac{\partial w}{\partial z} = 0. \tag{2.19a–c}$$

The dimensionless inlet and outlet pressures are derived by applying (2.16) to (2.6), which gives

$$p_1 = 1 \quad \text{at } z = 0, \ x \in [0, s(0, t)], \tag{2.20a}$$
$$p_2 = 0 \quad \text{at } z = 1, \ x \in [m(1) + h, 1]. \tag{2.20b}$$

Applying the scalings (2.16) to the no-flow boundary condition (2.7) results in the loss of the no-slip information, and we are consequently left with the following dimensionless no-penetration boundary condition:

$$w_1 = 0 \quad \text{at } z = 1, \ x \in [0, s(1, t)], \tag{2.21a}$$
$$w_2 = 0 \quad \text{at } z = 0, \ x \in [m(0) + h, 1]. \tag{2.21b}$$

To enforce the no-slip condition would require us to rescale into the boundary layer regions near the end caps at $z = 0, 1$, but we expect this to have a small effect on the global flow. The scaled symmetry conditions (2.8) are

$$u_1 = 0, \quad \frac{\partial w_1}{\partial x} = 0 \quad \text{at } x = 0, \tag{2.22a}$$

$$u_2 = 0, \quad \frac{\partial w_2}{\partial x} = 0 \quad \text{at } x = 1. \tag{2.22b}$$

7

The dimensionless Darcy flow (from (2.11)) through the porous membrane and cake is given by

$$u_1 = \kappa \left[p_1(c, z, t) - p_2(m(z) + h, z, t) \right] \quad \text{at } x = s(z, t), \tag{2.23}$$

where the dimensionless permeance is

$$\kappa = \left(\frac{1}{\kappa_m} + \frac{m - s}{k_c} \right)^{-1}, \tag{2.24}$$

which we note will evolve over time.

The outflow boundary condition at the membrane (2.12) becomes:

$$\phi_1^f u_1(s, z, t) = u_2(m + h, z, t), \tag{2.25}$$

and the no-slip condition (2.13), exploiting the small angle of the membrane, is

$$w_1 = 0 \quad \text{at } x = s(z, t), \tag{2.26a}$$

$$w_2 = 0 \quad \text{at } x = m(z) + h. \tag{2.26b}$$

Applying (2.16) to the cake-evolution equation (2.14) and taking the limit $\epsilon \to 0$ yields

$$\frac{\partial s}{\partial t} = -\phi_1^p u_1(s, z, t), \tag{2.27}$$

The corresponding initial condition for the cake position is

$$s(z, 0) = m(z). \tag{2.28}$$

2.4 Model reduction

The full dimensionless system is given by the lubrication equations (2.19) with boundary conditions (2.20)–(2.26) for each subdomain together with the blocking dynamics described by (2.27)–(2.28). The momentum equation in the x-direction (2.19a) gives $p_1 = p_1(z, t)$ and $p_2 = p_2(z, t)$.

In the inflow region Ω_1, the lubrication equations (2.19b,c) together with the symmetry boundary condition (2.22a) and the condition ensuring no-slip on the cake front (2.26a) can be manipulated to give the velocities in terms of the pressure:

$$u_1 = \tfrac{1}{2} x \left[(p_1' s^2)' - \tfrac{1}{3} x^2 p_1'' \right], \tag{2.29a}$$

$$w_1 = \tfrac{1}{2} p_1'(x^2 - s^2), \tag{2.29b}$$

where $'$ denotes partial differentiation with respect to z. Using (2.29a) in the Darcy flow boundary condition (2.23) we derive the following equation linking the pressures p_1 and p_2:

$$\tfrac{1}{3} \left(s^3 p_1' \right)' = \kappa \left(p_1 - p_2 \right). \tag{2.30}$$

The necessary boundary conditions for p_1 are supplied through the inlet pressure (2.20a) and no-flow condition at the closed end (2.21a):

$$p_1 = 1 \quad \text{at } z = 0, \tag{2.31a}$$

$$p_1' = 0 \quad \text{at } z = 1. \tag{2.31b}$$

We can derive the governing equation of motion for the pressure p_2 in Ω_2 in the same way. We first use the lubrication equations (2.19b,c) with the symmetry boundary condition (2.20b) and the no-slip condition on the membrane surface (2.22b) to derive

$$u_2 = \tfrac{1}{2}(x-1)\left[\left((m(z)+h-1)^2\right)'p_2' - \tfrac{1}{3}(x-1)^2 p_2''\right], \qquad (2.32a)$$

$$w_2 = \tfrac{1}{2}\left[(x-1)^2 - (m(z)+h-1)^2\right]p_2'. \qquad (2.32b)$$

The conservation-of-fluid-flux condition (2.25) with (2.32a) and the equation for p_1 (2.30) yield a second equation linking the pressures p_1 and p_2:

$$\tfrac{1}{3}\left[(m(z)+h-1)^3 p_2'\right]' = \phi_1^f \kappa\,(p_1 - p_2). \qquad (2.33)$$

The corresponding boundary conditions are derived from the outlet pressure (2.20b) and no-flow condition at the closed end (2.21b):

$$p_2 = 0 \quad \text{at } z = 1, \qquad (2.34a)$$

$$p_2' = 0 \quad \text{at } z = 0. \qquad (2.34b)$$

We can use these workings to rewrite the equations for the cake evolution (2.27) and (2.28) in terms of p_1 and p_2:

$$\frac{\partial s}{\partial t} = -\phi_1^p \kappa (p_1 - p_2), \quad s(z,0) = m(z). \qquad (2.35)$$

The problem is therefore reduced to solving the modified Reynolds equations (2.30)–(2.31) for p_1 in Ω_1 and (2.33)–(2.34) for p_2 in Ω_2 coupled with the permeance and cake-evolution equations given by (2.24) and (2.35) respectively. The remaining parameters in the system are the dimensionless midpoint a, angle β, permeance of the membrane κ_m, the cake permeability k_c, and the volume fraction of fluid ϕ_1^f in Ω_1. In practice the membrane is thin compared with the size of the filter module. We therefore consider the regular limit in which the dimensionless membrane thickness $h \to 0$ while the membrane permeance κ_m remains finite. This then removes the geometrical effect of membrane thickness while retaining its resistive properties.

The final reduced system of equations is:

$$\tfrac{1}{3}\left(s^3 p_1'\right)' = \kappa(p_1 - p_2), \qquad p_1|_{z=0} = 1, \quad p_1|_{z=1} = 0, \quad (2.36a)$$

$$\tfrac{1}{3}\left[(m(z)+h-1)^3 p_2'\right]' = \phi_1^f \kappa(p_1 - p_2), \quad p_2|_{z=1} = 0, \quad p_2'|_{z=0} = 0, \quad (2.36b)$$

$$\kappa = \left(\frac{1}{\kappa_m} + \frac{m-s}{k_c}\right)^{-1}, \qquad (2.36c)$$

$$\frac{\partial s}{\partial t} = -(1-\phi_1^f)\kappa(p_1 - p_2), \quad s(z,0) = m(z), \quad (2.36d)$$

$$m = a + \beta\left(\tfrac{1}{2} - z\right). \qquad (2.36e)$$

The solution to the model (2.36) provides insight into the flow dynamics and is used to calculate key quantities including the flux of fluid through the filtration-module domain, which is defined by

$$Q(t) = \int_0^s \phi_1^f w_1|_{z=0}\,\mathrm{d}x = -\tfrac{1}{3}\phi_1^f\left(s^3 p_1'\right)|_{z=0}. \qquad (2.37)$$

The amount of fluid processed through the device is given by the throughput:

$$V(t) = \int_0^t Q(\tau)\, \mathrm{d}\tau. \tag{2.38}$$

In practice, practitioners will use a filtration membrane at a fixed pressure difference across the module until the flux through the membrane drops such that it is no longer economical to use the filter. We therefore define the end time T to be the time at which the *in silico* experiment is terminated due to the flux dropping below some critical value Q_c. A key quantity of interest in this paper will be $V(T)$, the total throughput achieved at the end time.

The key control parameters in the model (2.36) are ϕ_1^f, a, β, and κ_m. In this paper, we will study the effects of each of these control parameters in optimising the performance of the filter in turn. In Section 3 we examine how the inclusion of particles influences the flow dynamics in the filter. In Section 4 we study the effect of the angle and position of the membrane on caking in relation to optimising performance. In Section 5 we consider how a spatially varying permeance might be utilised to optimise filtration performance.

3 The effect of adding particles to the steady-state system

Previous work by Pereira et al. [2021] presents a full analysis of the particle-free steady-state flow through a concertinaed filtration membrane. In this section, we look at the effect of adding particles into the system by considering how the steady-state flow changes with the volume fraction of particles.

To isolate the effect of particle inclusion (i. e. the effect of changing ϕ_1^f) we focus our attention to a transverse membrane positioned in the centre of the domain, by setting $\beta = 0$ and $a = 0.5$. We further restrict our attention to a steady-state set-up that corresponds to a scenario where the particles are removed on contact with the membrane, so that $s(z,t) = m(z)$ and $\kappa = \kappa_m$. Our reduced parameter space then comprises the membrane permeance κ_m and the volume fraction of fluid in the inflow domain ϕ_1^f.

For a membrane of such characteristics operating in this steady state we can derive explicit analytic solutions to (2.36) for the pressure:

$$
\begin{aligned}
p_{10} &= \frac{1}{N} \left[a^3(1-a)^3 + a^6 \cosh(M) + (1-a)^6 \cosh(M(z-1)) \right. \\
&\qquad \left. + a^3(1-a)^3 \cosh(Mz) - a^3(1-a)^3 M(z-1)\sinh(M) \right], \quad (3.1a)
\end{aligned}
$$

$$
\begin{aligned}
p_{20} &= \frac{1}{N} \left[a^3(1-a)^3 + a^6 \cosh(M) - a^3(1-a)^3 \cosh(M(z-1)) \right. \\
&\qquad \left. - a^6 \cosh(Mz) - a^3(1-a)^3 M(z-1)\sinh(M) \right], \quad (3.1b)
\end{aligned}
$$

where

$$
\begin{aligned}
M &= \sqrt{\frac{3\kappa_m}{a^3} + \frac{3\kappa_m \phi_1^f}{(1-a)^3}}, \\
N &= \left[(a^6 + (1-a)^6 \right] \cosh(M) + a^3(1-a)^3 \left[2 + M\sinh(M) \right]. \quad (3.2)
\end{aligned}
$$

We consider the total flux (of particles and fluid) in the upstream subdomain Ω_1 at $t = 0$ defined by

$$Q_1 = \int_0^a w_1|_{z=0} \, \mathrm{d}x = -\tfrac{1}{3} \left(m^3 p'_{10} \right)|_{z=0}. \tag{3.3}$$

Similarly we can define the amount of fluid processed through the device by calculating the flux out of the downstream subdomain Ω_2:

$$Q_2 = \int_a^1 w_2|_{z=1} \, \mathrm{d}x = \tfrac{1}{3} \left((m-1)^3 p'_{20} \right)|_{z=1}. \tag{3.4}$$

From conservation of fluid we have $\phi_1^f Q_1 = Q_2$.
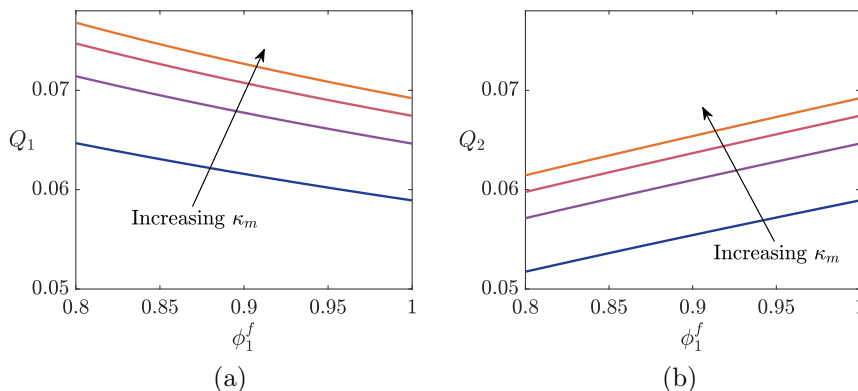
Figure 3: Analytical flux in Q_1 (3.3) in figure 3a and flux out Q_2 (3.4) in figure 3b plotted as functions of the fluid volume fraction for the case when $s(z,t) = m(z)$ and the particles are removed on contact with the membrane. Here, $\beta = 0$ and $a = 0.5$ and $\kappa_m = 0.5, 1, 1.5, 2$.

The analytical result for the steady fluxes as a function of the fluid volume fraction ϕ_1^f is shown in Figure 3. For a given applied pressure, as the volume fraction of fluid increases, the total flux of particles and fluid in Ω_1, Q_1, decreases but the total amount of fluid processed through Ω_2, Q_2, increases. Thus, the addition of particles in the system speeds up the flow in the upstream subdomain Ω_1, but decreases the total flux of fluid processed out of the device from Ω_2. We discuss this effect in further detail for a unidirectional flow in Appendix B in order to uncover the rationale for this observation. Furthermore, we also note that our results show that increasing the membrane permeance κ_m correspondingly increases the flux (figure 3), in agreement with physical intuition. This preliminary study shows that, even before blocking occurs, the initial system of fluid and particles is fundamentally different to the particle-free case.

In this section, we have studied the effect of introducing particles to a concertinaed filter operating in steady state. We now extend our study to explore the effects of control parameters governing the membrane configuration and their effect on the dynamic cake evolution in relation to optimal filtration performance.

4 The effect of membrane configuration

In this section, we assess the effect of angling and shifting the position of the membrane on the dynamic flux and throughput within the device. As we seek to study the effect of the configuration (namely the parameters a and β), for definiteness we shall assume a constant inflow fluid volume fraction $\phi_1^f = 0.8$, and a constant uniform membrane permeance and cake permeability, $\kappa_m = k_c = 1$, throughout this section.

4.1 The effect of membrane angle in relation to the total throughput and end time

We first explore the effect of angling the membrane. As such, we fix the remaining parameters, fix the membrane mid-point to be centred in the domain by setting $a = 0.5$, and vary β. We solve the governing system of equations (2.36) numerically using MATLAB's bvp4c solver, stepping forward in time until the flux Q (2.37) drops below the critical value Q_c which we take to be $Q_c = 10^{-2}$; this stopping criterion defines the end time T of the simulation.

The resulting cake-evolution profiles for different membrane angles are shown in Figure 4. We find that angling the membrane has a significant effect on the cake evolution. For a straight membrane with $\beta = 0$, the cake growth predominantly occurs at the domain edges, with the growth at the inlet $z = 0$ occurring faster than that at $z = 1$ (figure 4a). The total throughput is $V(T) = 0.29$ and is achieved at $T = 6.9$. For a slightly angled membrane ($\beta = 0.4$), while the cake growth remains focused at the edges, we also observe growth around the centre of the membrane (figure 4b). The overall cake evolution occurs more uniformly than that for $\beta = 0$. The end time $T = 16.1$ is more than double that for $\beta = 0$, and the corresponding total throughput is also increased to $V(T) = 0.80$. Increasing the membrane angle further ($\beta = 0.8$) gives a distinct cake-evolution profile with the growth focused at the centre of the membrane; the corresponding end time $T = 37.1$ and total throughput $V(T) = 1.26$ are significantly larger than found to be for $\beta = 0$ and $\beta = 0.4$ (figure 4c). These results show that angling the membrane results in the flux remaining above Q_c for longer and thus prolonging the lifetime of the filter and increasing the amount of fluid processed by the filter.

4.2 The effect of membrane angle on the flux–throughput curve

In practice, a standard tool to analyse the performance of a filter is the visualisation of the flux (Q) and throughput (V) relationship over time. The classic interpretation of these visualisations is that concave curves, i.e. those for which $Q''(V) < 0$, correspond to blocking due to caking, and convex curves, i.e. those for which $Q''(V) > 0$, represent internal blocking [Griffiths et al., 2014]. We present the flux–throughput curves for varying membrane angles in figure 5a. For straight to slightly angled membranes the flux–throughput curve is clearly concave. For larger values of β, however, the curve becomes convex. We examine this effect more closely by test-
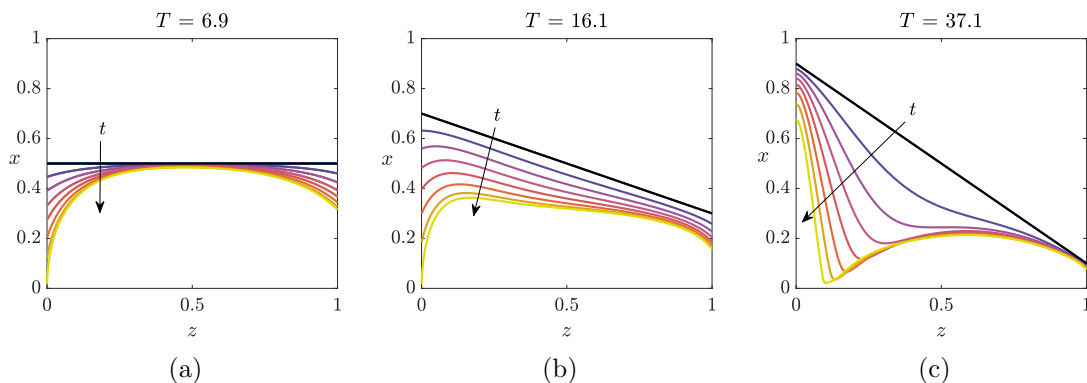
Figure 4: Evolution of the cake profile $s(z,t)$ over time found by solving (2.36) for $\beta = 0, 0.4, 0.8$ in figures 4a, 4b, and 4c respectively, with $a = 0.5$, $\phi_1^f = 0.8$, $\kappa_m = k_c = 1$, $Q_c = 10^{-2}$. The arrows indicated the direction of growth in time, and T is the end time at which the flux Q (2.37) drops below Q_c. Results shown for eight time steps equally spaced between $[0, T]$ for each angle tested.

ing the convexity as a function of the membrane permeance κ_m and angle β. We do this by fitting a second-order polynomial to the function $Q(V)$ to produce the interpolated flux function $\tilde{Q}(V)$. We then define the convexity measure by

$$C = \frac{d^2 \tilde{Q}}{dV^2}, \tag{4.1}$$

where $C < 0$ yields a concave function and $C > 0$ a convex function. Our results show that for small values of the membrane permeance the flux–throughput curves will remain concave for all values of β (figure 5b). For increased values of κ_m, however, the curves will be convex for larger values of β. Thus we find that, for certain sets of system parameters, the flux–throughput curves will be convex for blocking by caking only. These results show that interpreting the dominant blocking mechanism by the convexity of the flux–throughput curves can be inaccurate when the membrane is angled.

4.3 The optimal membrane configuration

We now investigate the effect of additionally shifting the membrane (i.e. varying a), with the objective of obtaining the optimal membrane configuration according to a given requirement. We explore the full angle domain $\beta \in [0, 1]$ and position domain $a \in [\beta/2, 1 - \beta/2]$. We seek numerical solutions but note that when either end of the membrane is close to a corner of the domain, the behaviour is difficult to resolve numerically. Thus, we slightly reduce our parameter domain to $\beta \in [0, 1 - \delta_\beta]$ and $a \in [\beta/2 + \delta_a, 1 - (\beta/2 + \delta_a)]$ for some small $\delta_\beta, \delta_a > 0$, and extrapolate our results to the full domains. For the results presented in this section we take $\delta_\beta = 0.05$ and $\delta_a = 0.01$.

There are various performance measures associated to filtration optimisation with the choice of measure depending on the industrial application. We choose to focus our attention to maximising the total throughput $V(T)$ and the average
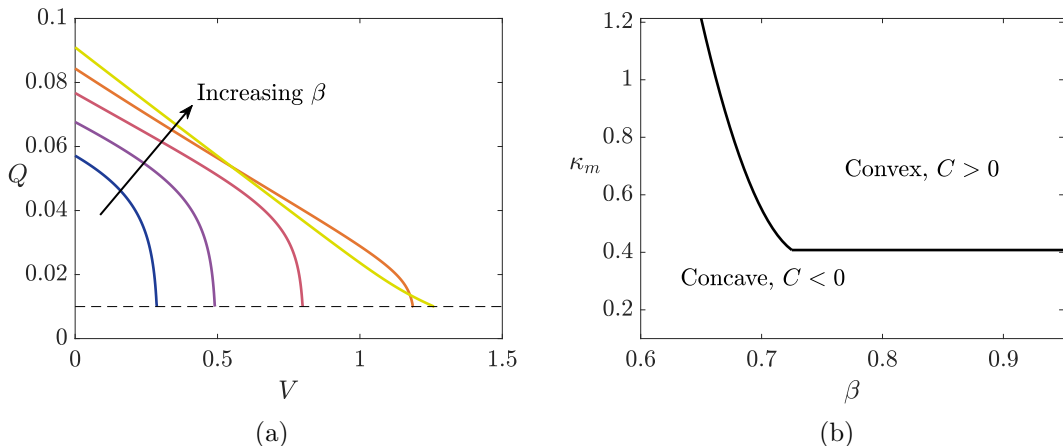
Figure 5: Flux–throughput curve resulting from solving the system of equations (2.36) and calculating the flux Q (2.37) and throughput V (2.38) for $a = 0.5$, $\phi_1^f = 0.8$, $\kappa_m = 1$, $Q_c = 10^{-2}$, and $\beta = 0, 0.2, 0.4, 0.6, 0.8$ in figure 5a. Convexity C (4.1) of the flux–throughput curves indicated through $\mathrm{sgn}(C)$ in the (κ_m, β) domain in figure 5b.

flux $\overline{Q}(T) = V(T)/T$. Note that since the instantaneous flux decreases in time, maximising $\overline{Q}$ corresponds to maximising the amount of fluid processed over the shortest time period. To examine how the optimal configuration depends on the choice of metric, we also consider a one-parameter family of measures in the form of a convex combination of the two metrics: $E(\alpha) = \alpha V(T) + (1 - \alpha)\overline{Q}(T)$ for some constant $\alpha \in [0, 1]$. While we present results for the chosen metrics only, the model presented in this paper can be used for any choice of optimisation metric.

We show results for our performance metrics in figure 6. We see that the total throughput is minimised for a horizontal membrane with $\beta = 0$ positioned towards the top and bottom of the domain, where $a = 1$ and $a = 0$ respectively (figure 6a). This corresponds to a filtration device in which the concertinaed membranes are close to touching. The maximum total throughput is achieved for $\beta \approx 0.2$ and $a \approx 0.7$ where the membrane is slightly angled and positioned off-centre upwards towards $x = 1$ (figure 6a). The average flux is similarly minimised when $a = 0$ or 1 and the concertina pleats close up. The average flux is maximised for $\beta \approx 0.7$ and $a \approx 0.4$. This is associated to membranes significantly angled and positioned off-centre towards the lower boundary at $x = 0$.

The distinction between the configurations that maximise $V(T)$ and $\overline{Q}$ is made clear when we consider the configurations that maximise $E(\alpha)$ (figure 6c). Our results show that the two optimal configurations discussed above are the only optimal configurations for $\alpha \in [0, 1]$. For small values of α the optimal configuration agrees with that which maximises the average flux. As the value of α is increased, the optimal configuration switches at (and remains fixed for all values of α greater than) the critical value of $\alpha \approx 0.02$ to coincide with the configuration that maximises the total throughput. The critical value of $\alpha \approx 0.02$ is notably small since there is a large difference between the magnitudes of the metrics $V(T)$ and $\overline{Q}$. Thus

14

we conclude that for particular applications for which it is preferable to maximise
the total amount of fluid processed, irrespective of the time it takes, the optimal
configuration is a slightly angled membrane positioned off-centre upwards towards
$x = 1$. For applications where it is important to maximise the amount of fluid
processed whilst minimising the time of operation, the optimal configuration is a
membrane that is significantly angled and positioned off-centre towards the lower
boundary at $x = 0$. The optimal angle and position in both cases are provided by
our model.

(a)

(b)

(c)
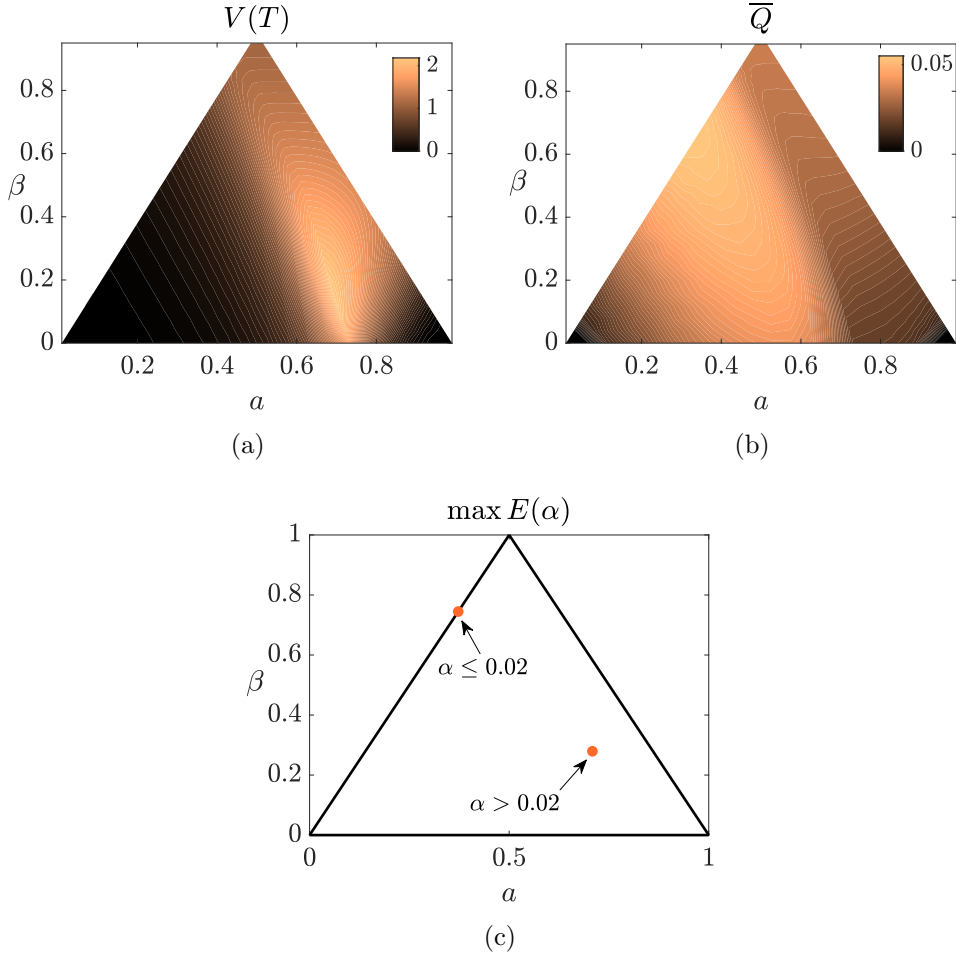
Figure 6: The total throughput $V(T)$ (2.38) in figure 6a, $\overline{Q} = V(T)/T$ in figure
6b, and the configuration that maximises $E(\alpha) = \alpha V(T) + (1 - \alpha)\overline{Q}$ in figure 6c
calculated from numerical solutions to (2.36) with $\beta \in [0,1]$, $a \in [\beta/2, 1 - \beta/2]$,
$\kappa_m = 1$, $\phi_1^f = 0.8$, and $Q_c = 10^{-2}$.

5 The effect of a spatially varying permeance

We have so far considered a constant membrane permeance κ_m. In this section we
relax this assumption to investigate the effect of a spatially varying permeance. This
is motivated by the observation that a spatially varying permeance may be chosen

15

to ensure uniform cake growth. A non-uniform permeance could be achieved by varying the membrane thickness in space or equally the pore distribution. The latter of these is becoming increasingly achievable through new technologies that enable practitioners to engineer a non-uniform pore distribution. This will minimise the effect of the changing geometry on introducing resistance to the flow. We therefore seek the membrane permeance profile that leads to uniform cake growth.

Although, in theory, we can derive the membrane permeance $\kappa_m(z, t)$ that yields uniform cake growth for all time, in practice it is difficult to vary the permeance in time. Therefore we choose to find the time-steady permeance $\kappa_m(z)$ that yields uniform cake growth initially. This is achieved for a permeance profile that generates a constant flow at the membrane front at $t = 0$:

$$u_1(x, z, 0) = \text{constant} = U_m \quad \text{at} \quad x = m(z). \tag{5.1}$$

Initially, $s(z, 0) = m(z)$ and so $\kappa(z, 0) = \kappa_m(z)$ using (2.36c). Using (5.1) in the Darcy-flow boundary condition (2.23) at the membrane, and noting that we have $p_i = p_i(z, t)$ for $i = 1, 2$ from the lubrication equations (2.19a), we then find

$$\kappa_m(z) = \frac{U_m}{p_1(z, 0) - p_2(z, 0)}. \tag{5.2}$$

We then use (5.2) to simplify the governing equations for the pressure (2.36a)–(2.36b), which decouple to give

$$\frac{1}{3}\left[m(z)^3 p_1'(z, 0)\right]' = U_m, \qquad p_1|_{z=0} = 1, \quad p_1'|_{z=1} = 0, \tag{5.3a}$$

$$\frac{1}{3}\left[(m(z) + h - 1)^3 p_2'(z, 0)\right]' = \phi_1^f U_m, \quad p_2|_{z=1} = 0, \quad p_2'|_{z=0} = 0. \tag{5.3b}$$

Equations (5.3) admit exact analytical solutions for p_1 and p_2:

$$p_1(z, 0) = 1 + \frac{12 U_m z \left[2a(z - 2) + \beta(3z - 2)\right]}{(2a + \beta)^2 (2a + \beta - 2\beta z)^2}, \tag{5.4a}$$

$$p_2(z, 0) = \frac{12 U_m (z - 1)\phi_1^f \left[2a(z + 1) + \beta - (3\beta + 2)z - 2\right]}{(-2a + \beta + 2)^2 (2a + \beta - 2\beta z - 2)^2}. \tag{5.4b}$$

From (5.2) we see that if there exists a zero pressure difference $\Delta p = p_1 - p_2 = 0$ anywhere along the membrane there will be an infinite permeance at that point, which corresponds to physical holes in the membrane. Note that we have introduced the, so far, unspecified parameter U_m. For each position and angle (a, β) there exists a bounded range of values of U_m for which $\Delta p > 0$, calculated from (5.4) for all z. We first note that U_m is bounded from below by $U_m = 0$ for which $p_1 = 1$ and $p_2 = 0$ from (5.4). To find an upper bound, we find the maximum value of U_m for which $\min \Delta p > 0$ holds at $t = 0$:

$$U_m^*(a, b) = \max U_m \quad \text{for which} \quad \Delta p(z, 0; a, b) > 0 \quad \text{for all } z. \tag{5.5}$$

This gives the bounded range $U_m \in [0, U_m^*]$ for each (a, β)-pairing. The contour plot for U_m^* in $\beta \in [0, 1 - \delta_\beta]$ and $a \in [\beta/2 + \delta_a, 1 - (\beta/2 + \delta_a)]$ for $\delta_\beta = 0.1$ and $\delta_a = 0.04$ is given in figure 7a. We see that for a membrane positioned towards the corners
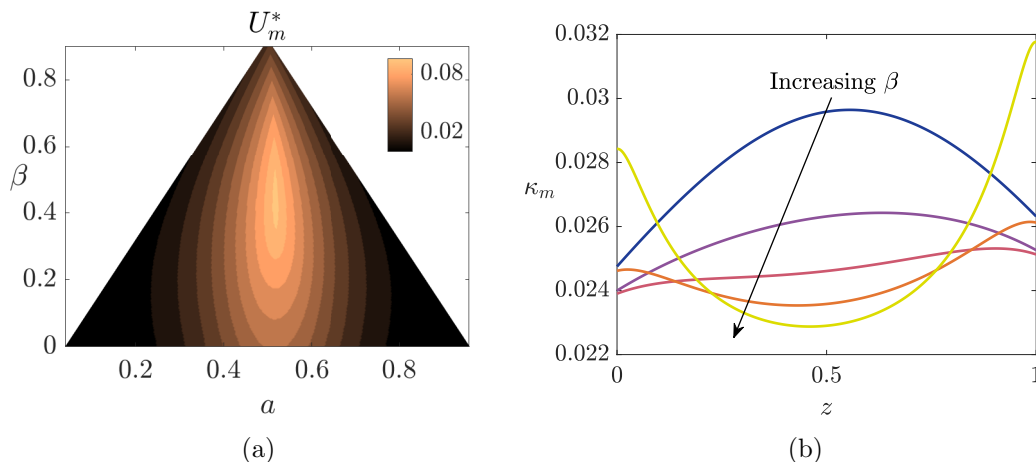
Figure 7: The upper bound of the constant velocity U_m^* calculated in (5.5) using analytical pressure profiles (5.4) and $\beta \in [0, 1]$ and $a \in [\beta/2, 1 - \beta/2]$ given in figure 7a. The non-uniform membrane permeance profiles $\kappa_m(z)$ (5.2) calculated using (5.4) with $\beta = 0, 0.2, 0.4, 0.6, 0.8$ at $t = 0$ in figure 7b for $a = 0.5$ and $U_m = 0.02$. Both figures use $\phi_1^f = 0.8$.

of the domain a very slow flow $U_m^* \ll 1$ is required for $\Delta p > 0$. For more centred membranes ($a \approx 0.5$), $\Delta p > 0$ can be achieved for faster flows. However, crucially, for the full (a, β)-parameter space tested, U_m^* is a small parameter, and thus uniform cake growth is only achieved for small fluxes through the domain.

We present the resulting permeance profiles $\kappa_m(z)$ in figure 7b for a range of membrane angles. We see that for horizontal and slightly angled membranes the permeance profile that ensures constant velocity at the membrane is concave. What this means in practice is that for horizontal (or close to horizontal) membranes, for constant velocity at the membrane, we should choose a membrane that has increased permeance at the centre of the membrane. As we increase the angle of the membrane the concavity of the permeance profile decreases, and for significantly angled membranes the membrane profile is strongly convex. In this case, we should therefore increase the permeance at the edges of the membrane and decrease the permeance towards to the centre.

6   Conclusions

We have examined caking dynamics in a concertinaed ceramic filtration membrane. Our work builds on the previous work of Pereira et al. [2021], which presented a study of the steady particle-free flow through a concertinaed filtration membrane. In this paper, we further developed the model to study the flow of a particle-laden fluid mixture through the same filtration device and derive the appropriate model for external cake build-up on the membrane surface. We modelled the flow of the fluid mixture on either side of the membrane using the Stokes equations and the flow through the porous membrane and cake layers using Darcy's law. By systematically reducing the model equations, we simplified the flow problem to solving

coupled lubrication equations, which account for the moving boundary associated with blocking, in the upstream and downstream subdomains on either side of the membrane.

Practitioners use flux–throughput curves to determine the nature of blocking within a filter, with concave and convex curves identified, respectively, with caking and internal blocking. We found, however, that when a centred membrane is angled caking dynamics can result in a convex flux–throughput curve. This result highlights potential misinterpretations that may result from using these curves to identify the governing blocking mechanism.

The overarching aim of this paper is to understand the effect of the membrane configuration on the filtration performance, which is determined by the particular measure of choice. As this metric will vary for different industrial applications, we consider a one-parameter family of metrics in this paper. The two extreme points of this family correspond to maximisation of the total throughput and average flux, respectively, while points in between correspond to linear combinations of the two properties. For the particular set-up of an infinitely thin membrane with unit permeance, the configuration that maximises the total throughput is a slightly angled membrane positioned off-centre upwards in the filtration-module domain. This configuration is distinct to that which optimises the average flux, which is a significantly angled membrane positioned off-centre towards the lower boundary of the domain.

We also explored the derivation of a spatially varying permeance corresponding to an initially uniform cake growth. We found that, to ensure a uniform cake growth, one requires a very small flux through the device initially. Thus, in practice, a non-uniform permeance will not be a useful tool when maximising the average flux through the domain (and consequently nor will it be useful to maximise the total throughput), but it may be relevant for different optimisation metrics.

In this paper we have introduced a mathematical framework for modelling caking in a direct-flow filtration device. Smart Separations Ltd are a start-up company who develop a direct-flow filtration device similar to that discussed in this paper. Motivated by insight provided by this company, we focused on the effect of caking dynamics on filtration performance. An interesting extension of the work presented here would be to explore the additional blocking mechanism of internal blocking.

The model formulation and results presented in this paper may be readily used by practitioners: for a specified application, this work provides understanding of the device configuration that optimises filtration performance.

7 Acknowledgements

A   Appendix

The cake front is an interface separating the upstream domain $\hat{\Omega}_1$ and the cake layer $\hat{\Omega}_c = \{\hat{x} \in [\hat{s}(\hat{z}, \hat{t}), \hat{s}(\hat{z}, \hat{t}) + \hat{h}], \hat{z} \in [0, 1]\}$. The position of this interface can be given implicitly by $\hat{F}(\hat{x}, \hat{z}, \hat{t}) = \hat{x} - \hat{s}(\hat{z}, \hat{t}) = 0$. The normal velocity of this moving boundary $\hat{v}_n := \hat{\boldsymbol{v}} \cdot \boldsymbol{n}_s$ can be written as

$$\hat{v}_n = -\frac{\partial \hat{F}/\partial \hat{t}}{|\boldsymbol{\nabla} F|}. \tag{A.1}$$

Imposing conservation of flux across this moving boundary yields

$$\hat{\boldsymbol{Q}}_1 \cdot \boldsymbol{n}_s - \hat{v}_n \hat{c}_1 = \hat{\boldsymbol{Q}}_c \cdot \boldsymbol{n}_s - \hat{v}_n \hat{c}_c, \tag{A.2}$$

where $\hat{\boldsymbol{Q}}_1$ and $\hat{\boldsymbol{Q}}_c$ are the particle fluxes within the upstream and cake domains, respectively, and $\hat{c}_1$ and $\hat{c}_c$ are the concentrations of particles within the upstream and cake domains, respectively.

The concentration of particles in $\hat{\Omega}_1$ and $\hat{\Omega}_c$ are related through

$$\frac{\hat{c}_c}{\phi_c^p} = \frac{\hat{c}_1}{\phi_1^p}, \tag{A.3}$$

where ϕ_c^p and ϕ_1^p are, respectively, the volume fractions of particles in Ω_c and in Ω_1. We have taken the intrinsic particle volume to be the same value in both phases. Neglecting diffusion in $\hat{\Omega}_1$, we can write the particle flux as $\hat{\boldsymbol{Q}}_1 = \hat{c}_1 \hat{\boldsymbol{u}}_1$. Moreover, we assume particles are not advected within the cake layer, and hence $\hat{\boldsymbol{Q}}_c = \boldsymbol{0}$. Using these values for the particle fluxes in (A.2), together with (A.3), we obtain the following expression for the normal velocity of the cake layer in terms of the system variables

$$\hat{v}_n = -\frac{\phi_1^p}{\phi_c^p - \phi_1^p} \hat{\boldsymbol{u}}_1 \cdot \boldsymbol{n}_s. \tag{A.4}$$

Substituting $\hat{v}_n$ (A.4) into (A.1) and rewriting in terms of the cake front position $\hat{s}(\hat{z}, \hat{t})$ gives (2.14) which, together with the initial condition (2.15), yields the cake evolution equation.

B   Appendix

In this appendix we consider a unidirectional pipe flow and include a porous membrane in the middle of the domain. The aim of this study is to understand the effect to the flow when particles are added to a system. We consider a unidirectional pipe flow to enable analytical insight.

We consider a cylindrical pipe of radius $\hat{R}$ and length $\hat{Z}$ as shown in figure 8. We assume axisymmetry and use cylindrical coordinates $(\hat{r}, \hat{z})$ to specify the geometry: we position a porous membrane of thickness $\hat{h}$ centred along the pipe at $\hat{z} = \hat{L}$, where $\hat{Z} = 2\hat{L} + \hat{h}$; the domain is then divided into the upstream and downstream subdomains

$$\hat{\Omega}_1 = \{\hat{r} \in [0, \hat{R}], \hat{z} \in [0, \hat{L}]\}, \tag{B.1a}$$
$$\hat{\Omega}_2 = \{\hat{r} \in [0, \hat{R}], \hat{z} \in [\hat{L} + \hat{h}, \hat{Z}]\}. \tag{B.1b}$$

The fluid mixture is made up of a continuous fluid phase and discrete particles to be filtered. We assume a constant volume fraction of fluid ϕ_1^f and volume fraction of particles $\phi_1^p = 1 - \phi_1^f$ in Ω_1. We further assume that there is perfect filtration by the membrane such that the downstream subdomain Ω_2 comprises only the fluid phase and as such the volume fraction of fluid is $\phi_2^f = 1$.
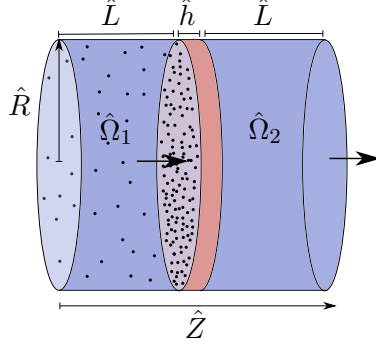

Figure 8: Schematic of the dimensional unidirectional pipe flow through a membrane. Particles are filtered out by the membrane drawn in pink in the centre of the pipe.

The flow is driven by a fixed pressure drop across the pipe $\Delta\hat{p} = \hat{p}_{\text{in}} - \hat{p}_{\text{out}} > 0$, with $\hat{p} = \hat{p}_{\text{in}}$ at $\hat{z} = 0$ and $\hat{p} = \hat{p}_{\text{out}}$ at $\hat{z} = \hat{Z}$. We denote the distinct pressure drops across $\hat{\Omega}_1$, the membrane, and $\hat{\Omega}_2$ by $\Delta\hat{p}_1$, $\Delta\hat{p}_m$, and $\Delta\hat{p}_2$, respectively. The total pressure drop across the pipe is therefore

$$\Delta\hat{p} = \Delta\hat{p}_1 + \Delta\hat{p}_m + \Delta\hat{p}_2. \tag{B.2}$$

We assume a steady, laminar, incompressible Poiseuille flow in $\hat{\Omega}_1$ and $\hat{\Omega}_2$, and can therefore express the total inflow flux of fluid and particles $\hat{Q}_1$ in $\hat{\Omega}_1$ and total outflow flux of fluid $\hat{Q}_2$ in $\hat{\Omega}_2$ in the following way:

$$\hat{Q}_1 = \frac{\pi \hat{R}^4 \Delta\hat{p}_1}{8\hat{\mu}\hat{L}}, \tag{B.3a}$$

$$\hat{Q}_2 = \frac{\pi \hat{R}^4 \Delta\hat{p}_2}{8\hat{\mu}\hat{L}}. \tag{B.3b}$$

Furthermore, we prescribe Darcy flow across the membrane to write the flux through the membrane as:

$$\hat{Q}_m = \pi \hat{R}^2 \hat{\kappa}_m \Delta\hat{p}_m, \tag{B.4}$$

where $\hat{\kappa}_m$ is the permeance of the membrane.

We nondimensionalise the system by introducing the following scalings:

$$\hat{r} = \hat{R}r, \quad \hat{z} = \delta\hat{R}z, \quad \hat{p} = \frac{\hat{\mu}\hat{W}}{\delta^2\hat{L}}p + \hat{p}_{\text{out}}, \quad \hat{\kappa}_m = \frac{\hat{R}^2}{8\hat{L}\hat{\mu}}\kappa_m,$$

$$\hat{Q}_1 = \frac{\pi\hat{W}\hat{R}^2}{\delta^4}Q_1, \quad \hat{Q}_2 = \frac{\pi\hat{W}\hat{R}^2}{\delta^4}Q_2, \quad \hat{Q}_m = \frac{\pi\hat{W}\hat{R}^2}{\delta^4}Q_m, \tag{B.5}$$

where $\delta = \hat{L}/\hat{R}$. Moreover, the velocity scaling $\hat{W}$ is given in terms of the pressure drop:

$$\hat{W} = \frac{\delta^2 \hat{L}}{\hat{\mu}} (\hat{p}_{\text{in}} - \hat{p}_{\text{out}}). \tag{B.6}$$

We choose a short wide domain with $\delta \ll 1$. This enables a closer comparison between the unidirectional flow system in this appendix and the non-unidirectional lubrication flow system presented in the body of the paper and discussed in Section 3.

Applying the scalings (B.5) to (B.3) and (B.4) yields the dimensionless fluxes in terms of the dimensionless pressure drops:

$$Q_1 = \Delta p_1, \quad Q_m = \kappa_m \Delta p_m, \quad Q_2 = \Delta p_2. \tag{B.7}$$

Using (B.7) in (B.3) together with conservation of fluid: $\phi_1^f Q_1 = Q_m = Q_2$ we can find the inflow and outflow fluxes in terms of the total pressure drop Δp:

$$Q_1 = \frac{\Delta p}{1 + \phi_1^f + \dfrac{\phi_1^f}{\kappa_m}}, \tag{B.8a}$$

$$Q_2 = \frac{\Delta p}{1 + \dfrac{1}{\phi_1^f} + \dfrac{1}{\kappa_m}}. \tag{B.8b}$$

The flux profiles are shown in figure 9. Analogously to the results in Section 3, the inflow flux decreases with increased fluid volume fraction (figure 9a). For a decreased fluid volume fraction, there is a corresponding increased particle volume fraction. There is consequently less physical space available for the fluid to move, so for the same fixed pressure drop, the flow will speed up. On the downstream side of the membrane we observe that the outflow flux increases with the fluid volume fraction (figure 9b). This shows that the total amount of fluid processed through the domain will increase when there are fewer particles in the system.
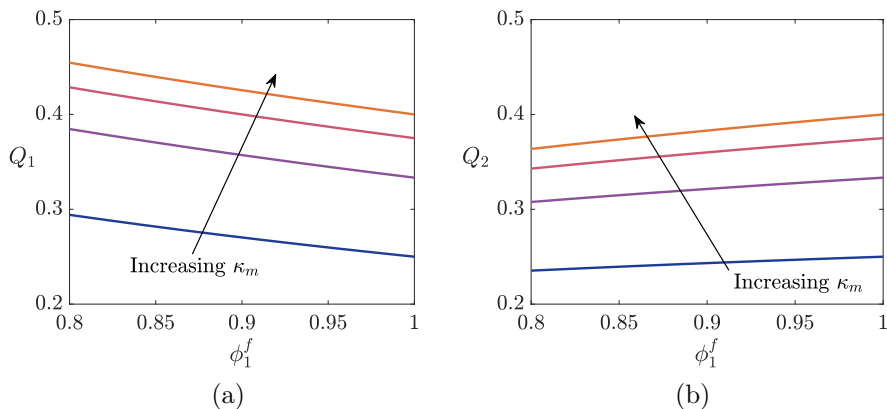

(a)

(b)

Figure 9: Analytical inflow flux (B.8a) and outflow flux (B.8b) through a pipe with dimensionless pressure drop $\Delta p = 1$ and porous membrane of permeance $\kappa_m = 0.5, 1, 1.5, 2$.

The results discussed in Section 3 and in this appendix show how including particles in the system affects the flux through a system of two open domains separated by a porous membrane for a given pressure drop. Namely, we find that introducing particles speeds up the flow rate upstream of the membrane whilst decreasing the total amount of fluid processed by the system.

References

G. S. Beavers and D. D. Joseph. Boundary conditions at a naturally permeable wall. *Journal of Fluid Mechanics*, 30(1):197–207, 1967.

I. M. Griffiths, P. D. Howell, and R. J. Shipley. Control and optimization of solute transport in a thin porous tube. *Physics of Fluids*, 25(3):033101, 2013.

I. M. Griffiths, A. Kumar, and P. S. Stewart. A combined network model for membrane fouling. *Journal of Colloid and Interface Science*, 432:10–18, 2014.

J. R. King and C. P. Please. Asymptotic analysis of the growth of cake layers in filters. *IMA Journal of Applied Mathematics*, 57(1):1–28, 1996.

R. D. Noble and S. A. Stern. *Membrane Separations Technology: Principles and Applications.* Elsevier, 1995.

V. E. Pereira, M. P. Dalwadi, E. Ruiz-Trejo, and I. M. Griffiths. Optimising the flow through a concertinaed filtration membrane. *Journal of Fluid Mechanics*, 913:A28, 2021.

P. Sanaei, G. W. Richardson, T. Witelski, and L. J. Cummings. Flow and fouling in a pleated membrane filter. *Journal of Fluid Mechanics*, 795:36–59, 2016.

Smart Separations Ltd. https://smartseparations.com/, 2020.

Y. Sun, P. Sanaei, L. Kondic, and L. J. Cummings. Modeling and design optimization for pleated membrane filters. *Physical Review Fluids*, 5(4):044306, 2020.

R. van Reis and A. Zydney. Bioprocess membrane technology. *Journal of Membrane Science*, 297(1-2):16–50, 2007.

M. Wang, S. Mondal, and I. M. Griffiths. The role of fouling in optimizing direct-flow filtration module design. *Chemical Engineering Science*, 163:215–222, 2017.

K. M. Yao, M. T. Habibian, and R. O'Melia. Water and waste water filtration. concepts and applications. *Environmental Science & Technology*, 5(11):1105–1112, 1971.